Review

A Review on Metal Oxide Semiconductor-Based Chemo-Resistive Ethylene Sensors for Agricultural Applications

Kongcan Hu, Yahan Cai, Ziru Wang, Zhengwei Zhang, Jieyu Xian [ID] and Cheng Zhang *

College of Engineering, Nanjing Agricultural University, Nanjing 210031, China;
2023812081@stu.njau.edu.cn (K.H.); caiyahan@stu.njau.edu.cn (Y.C.); 9213010726@stu.njau.edu.cn (Z.W.);
weizhzh@njau.edu.cn (Z.Z.); xianjy@njau.edu.cn (J.X.)
* Correspondence: zhangcheng@njau.edu.cn

Abstract: Ethylene, an important phytohormone, significantly influences plant growth and the ripeness of fruits and vegetables. During the transportation and storage of agricultural products, excessive ethylene can lead to economic losses due to rapid deterioration. Metal oxide semiconductor (MOS)-based chemo-resistive sensors are a promising technology for the detection of ethylene due to their low cost, high sensitivity, portability, etc. This review comprehensively summarizes the materials, fabrications, agricultural applications, and sensing mechanisms of these sensors. Moreover, the current challenges are highlighted and the potential solutions are proposed.

Keywords: metal oxide semiconductor; chemo-resistive sensor; ethylene sensor; agricultural detection

1. Introduction

Ethylene is an important phytohormone that has a major impact on the growth and ripeness of fruits, vegetables, and ornamental plants [1–4]. Most of the ethylene comes directly from plants and agricultural products [5]. For fruits and other ornamental cut flowers, the pathways of ethylene synthesis and the mechanisms of controlling ripeness have been extensively studied [6]. Some agricultural products produce excessive amounts of ethylene, which can lead to the rapid deterioration of agricultural products during transportation and storage, resulting in economic loss [7,8]. Precisely regulating ethylene levels in the environment helps keep agricultural products fresh. For plants, mature cells of seedlings, leaves, flowers, and roots of higher plants can produce ethylene [9]. Ethylene is closely associated with the processes of seed germination [10], cell elongation [11], fertilization [12], fruit ripeness [13], seed dispersal [14], pathogen defense [15], and stress response [1,16]. Even at low concentrations (0.01 ppm–1 ppm), the effect of ethylene on agricultural products can be observed. Therefore, precise detection of ethylene concentration is of great importance in the agricultural industry [17,18].

Gas chromatography (GC) is one of the most widely utilized and well-characterized analytical techniques used for the detection and quantification of ethylene [19]. Although GC displays a low detection limit, typically at the parts per billion (ppb) level, it requires complex measurement in the specific laboratory by professionals using specialized equipment, which hinders field monitoring of ethylene for agricultural products [20]. Optical ethylene sensors mainly utilize the light-absorption properties in the near-infrared region [19,21]. This method can achieve very low detection limits (less than 1 ppb) and rapid response speed (typically within seconds) [19,22,23]. However, expensive equipment hinders the wide application of this method, especially in agriculture [19]. Moreover, ethanol and acetaldehyde tend to interfere with the infrared measurement of ethylene [20]. Electrochemical gas sensors are based on the change in current from the redox reaction occurring between the electrode and the gas being analyzed. Despite the relatively low cost and accuracy of detection, their highly active electrodes are sensitive to interfering substances, resulting in poor selectivity [20]. Carbon nanotube (CNT) sensors detect the presence and

concentration of a gas by measuring the change in the conductivity of a carbon nanotube material when exposed to a gas. Despite its high sensitivity and selectivity, it is sensitive to environmental conditions, expensive to prepare, and insufficiently selective [24].

Compared to the conventional measurement methods, a metal oxide semiconductor (MOS)-based gas sensor is another promising technique [25], featuring low cost, high sensitivity, long service life, and portability [26,27]. When exposed to analyzed gases, the conductivity or dielectric constant of these materials changes. According to the detection principle, MOS-based ethylene sensors are categorized as chemo-capacitive or chemo-resistive types, which can convert the effects of ethylene action into capacitive or resistive signals, respectively [20,28–30]. Compared to chemo-capacitive sensors, chemo-resistive sensors offer the advantages of simpler structure and lower cost [31]. Moreover, chemo-resistive-based sensors can respond swiftly to changes in ethylene concentration and exhibit extended longevity, which can deliver a stable and reliable detection [32–39]. Thus, MOS-based chemo-resistive sensors have great potential for simple, rapid, and in-field detection of ethylene.

Herein, this article provides a comprehensive review of the materials, fabrications, applications in agriculture, and sensing mechanisms of MOS-based chemo-resistive sensors (Figure 1). In Section 2, we summarize the materials of the mainly used MOSs, tin dioxide (SnO_2) and zinc oxide (ZnO), and the others, as well as their fabrication methods, including chemical vapor deposition (CVD), ultrasonic spray pyrolysis (USP), sputtering, wet chemical method, and electrochemical deposition, reflux method, and hydrothermal method. In Section 3, we review the pioneer works of applying MOS-based chemo-resistive ethylene sensors in agriculture, mainly including ripeness monitoring of post-harvest fruits. In Section 4, we introduce the sensing mechanisms of n-type and p-type MOSs. Finally, we point out the existing limitations in this area, including low selectivity, poor limit of detection and high operation temperature, low anti-humidity capability, long-term instability, and sensor discreteness, as well as propose possible solutions such as structure engineering and doping.
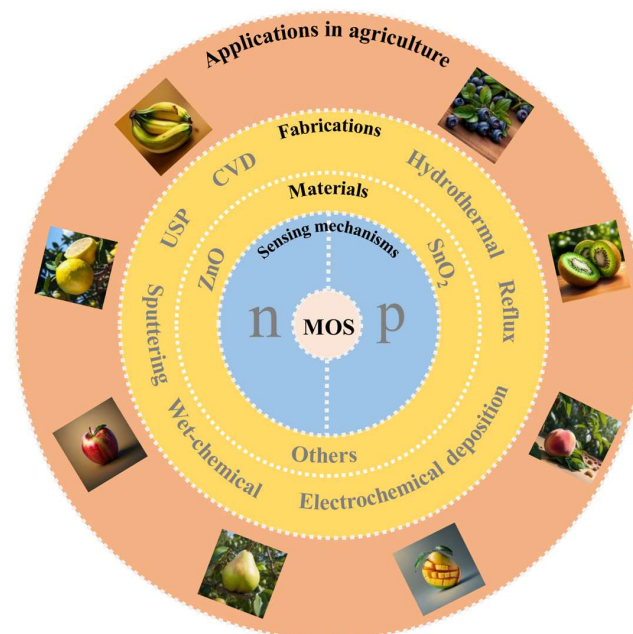

Figure 1. Structure of the review. The concentric layers from inner to outer, correspond to sensing mechanisms, materials, fabrication methods, and applications sequentially. The outermost layer indicates the application of sensors to these fruits.

2. Materials and Fabrications

MOSs used for ethylene sensors can be fabricated using multiple methods, such as CVD, USP, sputtering method, wet chemical method, electrochemical deposition, reflux

method, and hydrothermal method. In this section, we will review the fabrication methods for specific MOSs, including the two mainly used ones for ethylene sensors, SnO_2 and ZnO, and others. The fabricated gas sensors will be illustrated to demonstrate the features of the corresponding methods.

2.1. SnO_2

SnO_2 is the most prevalent sensing material used for ethylene sensors due to its high sensitivity [40], reliability, and electrical conductivity [41]. The common SnO_2 fabrication methods include CVD, USP, and sputtering methods.

2.1.1. CVD

CVD is a process that utilizes gaseous substances to chemically react on a solid and produce solid deposits. By regulating the conditions of CVD, the properties of products, such as film size, crystallinity, and number of layers, can be precisely controlled [42]. The produced film has the characteristics of high purity, high quality, and low defects. Moreover, it can also uniformly deposit materials on complex surfaces and microstructures, which is particularly important for microelectronics and nanotechnology applications [43,44].

The typical fabrication procedures of SnO_2 using CVD [45–47] are outlined as follows. In the initial step, Sn particles were deposited onto carbon fiber paper (CFP). Anhydrous $SnCl_2$ powder was positioned in a quartz boat placed at the center of a tube furnace, with CFP situated downstream to serve as a support for Sn particles. Subsequently, the samples underwent annealing under atmospheric conditions at 300 °C for 60 min to oxidize Sn into SnO_2 (Figure 2(ai)).
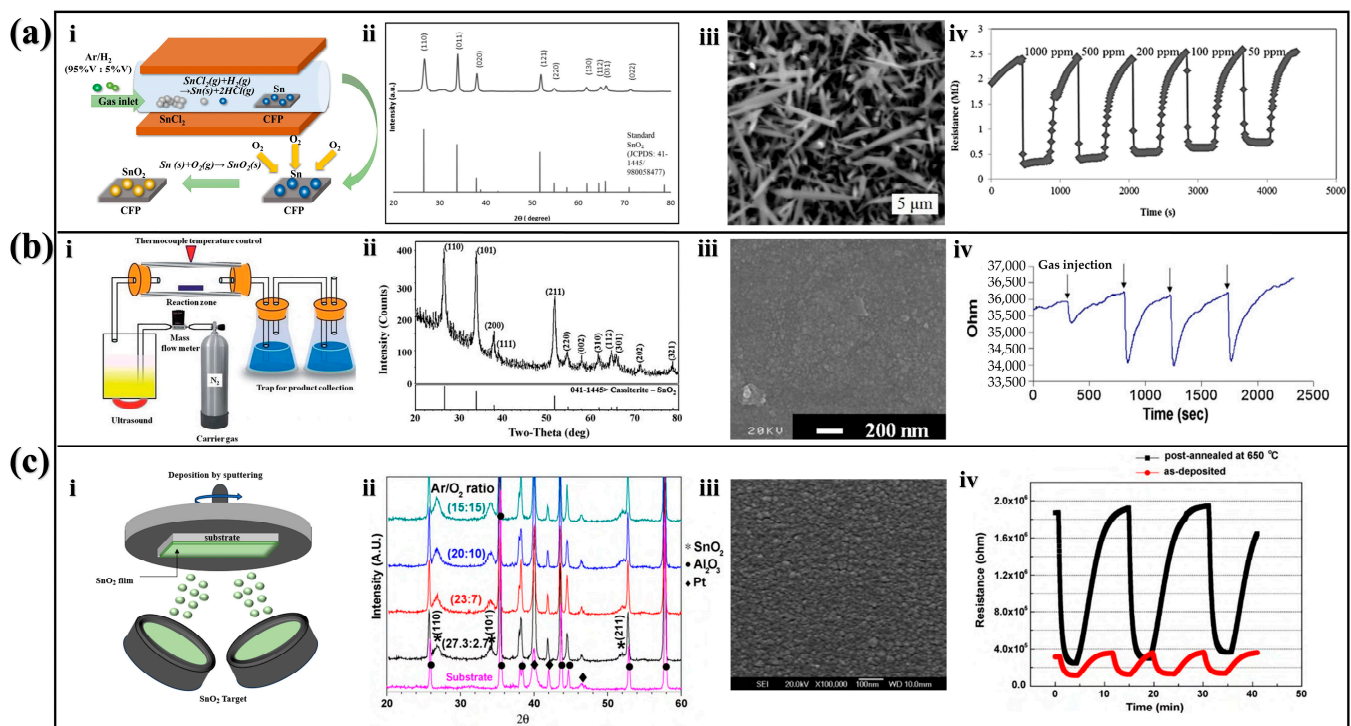

Figure 2. SnO_2 fabricated by different methods. (**a**) CVD method: (**i**) Schematic diagram of CVD process, (**ii**) XRD of the fabricated sample, (**iii**) SEM of the fabricated sample, and (**iv**) The response curve to different concentrations of ethylene [45]. (**b**) USP method: (**i**) Schematic diagram of the USP [48], (**ii**) XRD of SnO_2 thin film, (**iii**) SEM of SnO_2 thin film, and (**iv**) The response curve to different concentrations of ethylene [49]. (**c**) Sputtering method: (**i**) Schematic diagram of magnetron sputtering process, (**ii**) XRD of the fabricated SnO_2 thin film, (**iii**) SEM of the fabricated SnO_2 thin film, and (**iv**) The response curve to different concentrations of ethylene [50].

The chemical structure of the sample was characterized by X-ray diffraction (XRD). XRD spectra exhibit peaks such as (110), (011), and (121) corresponding to standard SnO_2 (ICSD # 98-005-8477) [45] (Figure 2(aii)). The result demonstrates that the fabricated samples are SnO_2 with a tetragonal rutile structure. The fabricated samples were characterized by scanning electron microscopy (SEM). The SEM shows the diameter of the fabricated SnO_2 nanowires is about 42 nm (Figure 2(aiii)) [45]. This structure has a high aspect ratio (L/D) and sufficient active sites for gas adsorption and desorption, which can increase the sensitivity of the sensor. The response characteristics of the sensor toward different concentrations of ethylene gas were investigated at the temperature of 450 °C (Figure 2(aiv)) [45]. It is evident that the resistance of the sensors sharply decreases upon exposure to ethylene and gradually increases after being exposed to air. This indicates that the sensor exhibits a relatively high response and good recovery to ethylene, proving the excellent performance of SnO_2 prepared by the CVD method.

2.1.2. USP

USP refers to the technology of droplet generation induced by ultrasound [51]. As a conventional deposition technique, it has been employed for the production of various nanostructures. USP presents advantages such as low cost, stable coatings, wide applicability, and great flexibility in a continuous process for synthesizing oxide materials [48].

The typical fabrication procedures of SnO_2 using the USP method [48,49] are as follows. The USP system consists of three main parts (Figure 2(bi)). An aqueous solution of $SnCl_4 \cdot 5H_2O$ was stirred for 20 min in a flask, and hydrochloric acid was subsequently added to create a homogeneous solution, which was then transferred to an ultrasonic transducer, where it was converted into an aerosol. Subsequently, this aerosol was conveyed into the reaction zone using N_2 as the carrier gas. Quartz substrates were positioned in the reaction zone, and the reaction proceeded for 2 h at 400 °C. The aerosol was then heated, vaporized, pyrolyzed, and sintered to obtain the final product.

As shown in Figure 2(bii), the peaks presented by the XRD of the samples match those of the standard SnO_2, proving that SnO_2 has a cassiterite structure. In addition, the sharp peaks prove that tin dioxide has good crystallinity, which contributes to the gas-sensitive properties. Using the Scherrer equation, the grain size of SnO_2 is calculated to be 15.2 nm, which can provide more surface area to improve sensitivity. An SEM image of the prepared SnO_2 is shown in Figure 2(biii) [49]. It reveals a uniform polycrystalline SnO_2 thin film. Moreover, SnO_2 exhibits a small crystal size, which could increase surface area, thus enhancing sensitivity. Compared to the thicker film sensor, this sensor can offer excellent unit-to-unit consistency and shorten stabilization time. They also tested the sensor's response to ethylene at 350 °C (Figure 2(biv)). The sensor resistance changes at a relatively fast rate and has good recovery, which indicates that the sensor prepared by this method has good performance.

2.1.3. Sputtering Method

Sputtering method uses a beam of inert gas ions to vaporize the solid, which is a common method to fabricate nanoparticle films [52]. The sputtered films are well combined with the substrate, and they also have high purity, good compactness, and uniformity. Moreover, the sputtering process has great repeatability, and the film with a uniform thickness can be obtained on a large area substrate [53].

The typical fabrication procedures of SnO_2 using sputtering method [50] are as follows. A SnO_2 ceramic target of 99.99% purity was subjected to radio-frequency (RF) sputtering at 80 W over 25 min, maintaining a total gas mixture flow rate at 30 sccm. Subsequent annealing was executed at 650 °C for 1 h in ambient air using a tube furnace. Before the SnO_2 deposition, a Pt electrode of 100 nm thickness was added to the alumina substrate via direct current. Using a shadow mask, an interdigitated layout was crafted, maintaining a 4 mm gap and width for the electrodes (Figure 2(ci)).

Figure 2(cii) shows the XRD spectra of the deposited films at different argon-to-oxygen ratios. The diffraction peaks of the substrate contain only the peaks of the Al_2O_3 substrate and the Pt electrode, while three characteristic peaks of (110), (101), and (211) corresponding to SnO_2 are observed on the deposited films. The surface topography of the prepared SnO_2 was analyzed (Figure 2(ciii)) [50]. It can be clearly seen that its structure is relatively complete and closely arranged, and there is no obvious crack. The advantage of this is that the obtained material has good stability, which also helps to improve the electrical conductivity. The gas response of the product is shown in Figure 2(civ) [50]. The measurement was conducted at 25 ppm ethylene concentration. The sensitivity values for post-annealed and as-deposited films are calculated to be approximately 6.5 and 2.7, respectively. It is evident that post-annealing can improve sensitivity, mainly attributed to the optimization of crystallization quality.

2.2. ZnO

ZnO is the other commonly used MOS for ethylene sensors. Besides excellent sensing performances, ZnO has high specific surface area, high crystallinity, high cost-effectiveness, and scalable production [54–58]. ZnO is widely fabricated by wet chemical method, electrochemical deposition, and sputtering method.

2.2.1. Wet Chemical Method

Wet chemical method is a common method, mainly including co-precipitation, hydrothermal method, and sol-gel method. This method begins with the dissolution of the oxide in a solvent, which is then precipitated or crystallized. Compared to other preparation methods, wet chemistry method usually does not require expensive equipment or complex operation, and the material properties can be relatively controlled. In addition, it also performs well in synthesizing complex structures and multi-component materials at relatively low cost [59].

The typical fabrication procedures of ZnO using wet chemical method are as follows [60]. As shown in Figure 3(ai), $Zn(CH_3COO)_2$ and $CO(NH_2)_2$ were dissolved in water and stirred for 1 h. The resulting transparent solution was enclosed in a conical flask and subjected to a 100 °C heating process for 6 h. Subsequently, the obtained products were cooled to ambient temperature, followed by centrifugation, washing, drying, and annealing [60].

The chemical structure of ZnO nanosheets is shown in XRD spectra (Figure 3(aii)). The peaks of the ZnO nanosheets correspond to those of the fibrillar zincite ZnO. In addition, the XRD spectra of the fabricated samples show weak Pd Peaks, proving the ZnO nanosheets are successfully doped with Pd. The SEM image of the obtained materials shows many randomly placed nanosheets with a large number of mesoporous pores (Figure 3(aiii)). A large number of mesoporous nanosheets can provide sufficient active sites, which contributes to the adsorption and detection of ethylene molecules and increases the sensitivity. The ethylene response of the prepared ZnO is plotted in Figure 3(aiv). The sensor could respond to the minimal concentration of 10 ppb. This low-limit detection is crucial for the monitoring of trace ethylene in the environment. When the ethylene concentration increased from 10 ppb to 1 ppm, the response also increased. The excellent sensing performance indicates the high quality of ZnO prepared using this method.
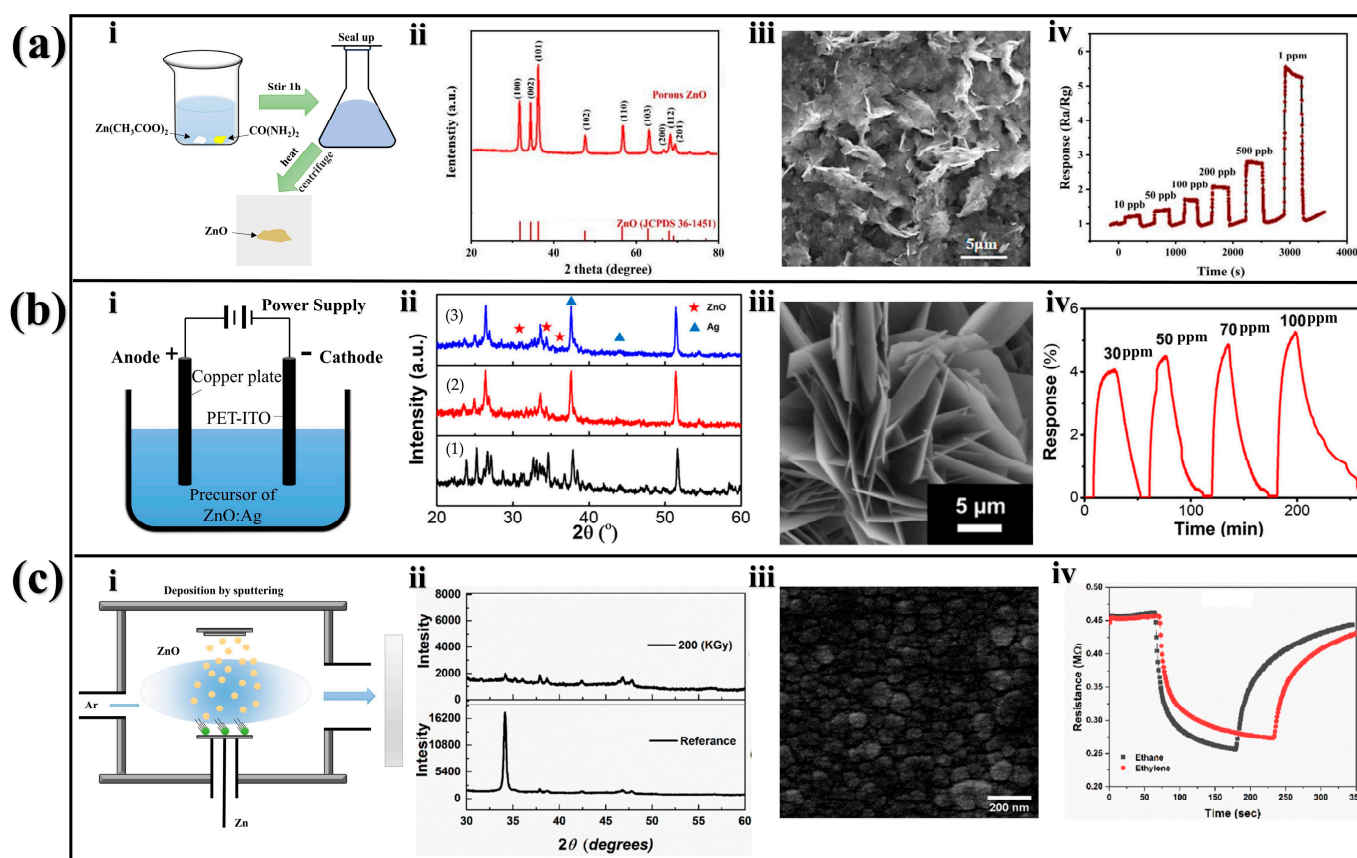
Figure 3. ZnO fabricated by different methods. (**a**) Wet chemical method: (**i**) Flow diagram of wet chemical method, (**ii**) XRD of the ZnO nanosheets, (**iii**) SEM of the ZnO nanosheets, and (**iv**) Real-time responses of the ZnO nanosheets to different concentrations of ethylene [60]. (**b**) Electrochemical deposition: (**i**) Schematic diagram of ZnO-Ag electrochemical deposition process, (**ii**) XRD of the obtained sample, (**iii**) SEM of the obtained sample, and (**iv**) The response curve of the sensor to ethylene [61]. (**c**) Sputtering method: (**i**) Schematic diagram of magnetron sputtering process, (**ii**) XRD of ZnO thin films, (**iii**) SEM of ZnO thin films, and (**iv**) Response curves of ZnO-based ethylene sensor to 1.2 ppm of ethylene (red dots) and to 1.2 ppm of ethane [62].

2.2.2. Electrochemical Deposition

Electrochemical deposition uses electrical energy to produce layers and usually involves the oxidation or reduction of highly soluble substances on the electrode surface [63]. The electrochemical deposition method offers the advantages of low-temperature conditions, high-throughput mass production, and low cost.

The typical fabrication procedures of ZnO nanorods using electrochemical deposition are as follows [61,64]. The whole preparation process is relatively simple (Figure 3(bi)). The substrates, comprising polyethylene terephthalate-indium doped tin oxide (PET-ITO), underwent a thorough sequential cleaning process. A precursor solution was formulated by combining equimolar proportions of $Zn(NO_3)_2 \cdot 4H_2O$ and $C_6H_{12}N_4$ in deionized water. Ag was introduced into the precursor through the addition of 0.5 mM $AgNO_3$. Then, the solutions were aged for a duration of 2 h. The electrodeposition procedure was carried out utilizing an electrical potential of -1.2 V at a temperature of 10 °C for a duration of 2 h.

The XRD of the samples doped with different percentages of silver is shown in Figure 3(bii). The positions of the ZnO diffraction peaks match with the ICSD number 98-016-3380. In addition, the diffraction peak of silver is located at $2\theta = 44°$, matching Miller index of (002). The result also shows that the diffraction peaks of silver are increasing with the increase in silver percentage. During electrodeposition, the ZnO-Ag structure shows (002), (010), and (011) multi-directional growth. Moreover, the higher amount of

Ag is quantitatively seen by the stronger Ag peaks in the ZnO-Ag0.6 and ZnO-Ag0.7 (Figure 3(bii,2) and Figure 3(bii,3)) than those of ZnO-Ag0.5 (Figure 3(bii,1)).The SEM image shows the obtained samples were nanosheets with thickness between 300 and 500 nm (Figure 3(biii)) [61]. Nanosheet structures usually have a large specific surface area, which helps to improve the reactivity of the material. The response of the sensor to ethylene is shown in Figure 3(biv). We can see that the response increases with the ethylene concentration. However, the response is relatively low, and the response time is on the minute scale, mainly due to the room temperature working conditions.

2.2.3. Sputtering Method

Sputtering method is also used in the preparation of ZnO. The advantages of this method have been described in the previous article, but the specific operation steps are different when used to prepare ZnO. The typical fabrication procedures of ZnO nanorods using sputtering method are as follows [62,65]. A film of ZnO with thickness of 300 nm was deposited from a ZnO target onto a substrate with interdigitated electrodes. Throughout the sputtering process, the substrate was secured onto a holder that rotated at 80 rpm and was positioned 3.5 cm away from the ZnO target. The deposition parameters were set at an input power of 100 W, a growth pressure at 3×10^{-3} Torr, and maintained argon gas flow of 10 sccm (Figure 3(ci)).

As shown in Figure 3(cii), the unirradiated sample exhibits a strong peak (002), which almost disappears after irradiation with 200 kGy. This is related to structural changes due to collisions between the incident radiation photons and the sample nuclei. The surface morphology of the obtained ZnO films is shown in Figure 3(ciii), which was relatively rough. ZnO with rough surface morphology usually has a larger specific surface area, which helps to improve the sensing performance. The response of the sensor to ethylene (red line) is shown in Figure 3(civ). Under atmosphere, the resistance of the sensor was stably maintained at a high level. When it was exposed to 1.2 ppm of ethylene at 350 °C, the resistance began to decrease until the saturation state. After being re-exposed to atmosphere, the resistance almost returned to the initial value. However, apart from ethylene, the ZnO sensor also demonstrated response to ethane (black line).

2.3. Other MOSs

In the previous sections, we have comprehensively summarized fabrication methods of the two commonly used MOSs for ethylene gas sensors. These materials and fabrication methods all have their advantages and disadvantages. In addition to SnO_2 and ZnO, TiO_2 [29], Fe_2O_3 [66], and Co_3O_4 [67] are also applied for ethylene sensors due to their decent sensing performance, non-toxicity, and stability [68]. They are fabricated in a slightly different way than SnO_2 and ZnO. Here, we introduce a typical preparation method for each of these three metal oxides.

2.3.1. TiO_2 Fabricated by Reflux Method

Reflux method is a synthetic chemical method commonly used in laboratory. It allows for prolonged control over temperature and pressure, contributing to the increased purity of the synthesized compounds. This method can also be very convenient to heat the solution. Reflux systems also prevent the loss of volatile compounds during the reaction, helping to maintain the concentration of reactants and enhance reaction efficiency.

The typical fabrication procedures of TiO_2 using reflux method are as follows (Figure 4(ai)) [29]. The apparatus used in the reflux method consists of a flask with a condenser. $TiCl_4$ is first mixed with distilled water. Then, ammonia water is added to the mixed solution and refluxed for 5 h to adjust the PH to 8–9. Finally, the sediment is filtered, washed, and dried.

The nano powders were characterized by XRD (Figure 4(aii)). The XRD pattern of TiO_2 confirms that the product has a single-phase property and a tetragonal structure. The particle size of TiO_2 was calculated as 33 nm using Scherrer equation. In addition, the

diffraction peak is very sharp, indicating that it has good crystallinity. The field emission scanning electron microscopy (FESEM) image of the prepared TiO_2 is shown in Figure 4(aiii). It has a monoclinic structure with a particle size of 27 nm. This structure can increase the surface area and thus improve the ethylene sensitivity.
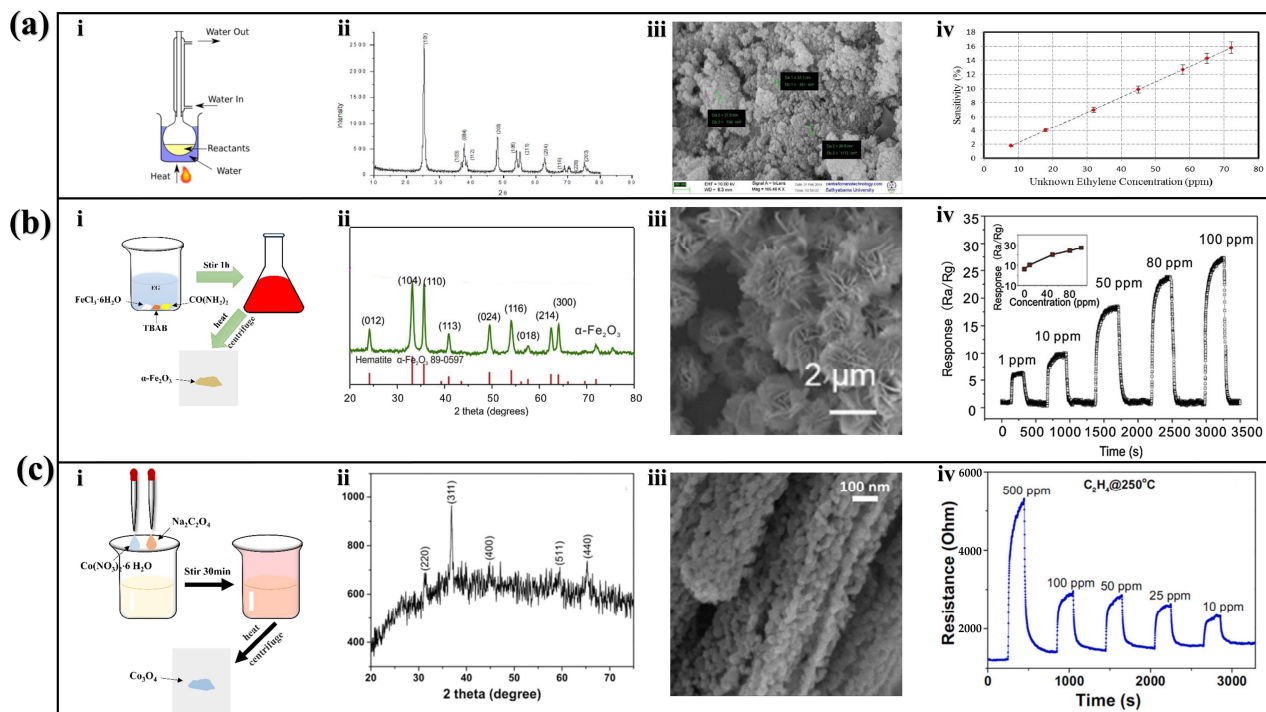

Figure 4. Other MOSs and their fabrication methods. (**a**) TiO_2 fabricated by reflux method: (**i**) Schematic diagram of reflux method, (**ii**) XRD of the TiO_2, (**iii**) FESEM of the TiO_2, and (**iv**) The sensitivity characteristics of the TiO_2 to different concentrations of ethylene at 250 °C [29]. (**b**) Fe_2O_3 fabricated by wet chemical method: (**i**) Flow diagram of wet chemical method, (**ii**) XRD of the obtained sample, (**iii**) SEM of the obtained sample, and (**iv**) Real-time responses of the α-Fe_2O_3 to different concentrations of ethylene [66]. (**c**) Co_3O_4 fabricated by hydrothermal method: (**i**) Flow diagram of hydrothermal method, (**ii**) XRD of the obtained sample, (**iii**) FESEM of thin films, and (**iv**) The gas response of the product to different concentrations of ethylene [69].

The sensing characteristics of the sensor toward different concentrations of ethylene gas were investigated at the temperature of 250 °C (Figure 4(aiv)). It can be seen from the response curve that the sensor shows good linearity in the measurement range. This allows the sensor to perform more consistently under different operating conditions, improving reliability and stability. Even when the ethylene concentration is less than 10 ppm, it still has a certain sensitivity. Although the number is not high, this is a problem that needs to be solved in the future. In summary, the sensor prepared by this method has good performance.

2.3.2. Fe_2O_3 Fabricated by Wet Chemical Method

Wet chemical method is also used in the preparation of Fe_2O_3. The advantages of this method have been described in the previous section, but the specific operation steps are different when used to prepare Fe_2O_3. The typical fabrication procedures of flower-like hierarchical porous α-Fe_2O_3 using the wet chemical method are as follows (Figure 4(bi)) [66]. First, 0.6 g of ferric chloride ($FeCl_3 \cdot 6H_2O$), 3.6 g of tetrabutylammonium bromide (TBAB), and 1.35 g of urea are added to 90 mL of ethylene glycol (EG). The resulting red liquid is then transferred to a flask and constantly stirred. The stirred mixture is heated to a boil, with continued stirring of boiling water for 20 min until the mixture turns green, indicating

that the reaction is complete. Finally, the green precipitate is washed, dried, and calcined to obtain the final product α-Fe$_2$O$_3$.

XRD patterns of α-Fe$_2$O$_3$ are shown in Figure 4(bii). The pattern of Fe$_2$O$_3$ shows many sharp peaks, which are highly correlated with hematite α-Fe$_2$O$_3$ (JCPDS No. 89-0597). Next, the surface topography of the prepared α-Fe$_2$O$_3$ was analyzed (Figure 4(biii)). Some flower-like hierarchies can be clearly seen from SEM. The structure is maintained from precursor to calcined porous Fe$_2$O$_3$, and it is self-assembled from ultra-thin nanosheets with a thickness of about 20 nm. The self-assembled flower-like layered porous α-Fe$_2$O$_3$ structure of these nanosheets has a high specific surface area, which can provide a larger adsorption area for ethylene and accelerate the diffusion of gas across the surface. Thus, the sensitivity of the sensor is improved. The real-time response curves of α-Fe$_2$O$_3$ to ethylene with concentration ranging from 1 to 100 ppm are shown in Figure 4(biv). Obviously, the gas sensor based on α-Fe$_2$O$_3$ exhibits notable sensitivity to ethylene, even within a low concentration range. At 1 ppm of ethylene exposure, the response (R_a/R_g) is 6. As the concentration rises, the response demonstrates an almost linear increase. The excellent response indicates the high quality of the sensor prepared by this method.

2.3.3. Co$_3$O$_4$ Fabricated by Hydrothermal Method

The hydrothermal method offers notable advantages over alternative approaches. It is particularly advantageous for generating nanomaterials that may not exhibit stability at elevated temperatures. The hydrothermal method allows for the production of nanomaterials characterized by high vapor pressures, minimizing material loss. Additionally, the hydrothermal synthesis process enables precise control over the composition of the synthesized nanomaterials through liquid-phase or multiphase chemical reactions.

The typical fabrication procedures of Co$_3$O$_4$ using hydrothermal method are as follows (Figure 4(ci)) [69]. A solution is formulated by dissolving cobalt (II) nitrate hexahydrate (Co(NO$_3$)$_2$·6 H$_2$O) and sodium oxalate (Na$_2$C$_2$O$_4$) in a blend of deionized water and ethylene glycol with a water-to-ethylene glycol ratio of 1:2. This process yields a pinkish transparent solution. The prepared solution is then sterilized, heated, and cooled to room temperature. It is then centrifuged, washed, dried, and annealed to obtain the final product.

The chemical structure of the sample was characterized by XRD (Figure 4(cii)). The primary peaks observed in the XRD pattern corresponded to the crystallographic planes (220), (311), (400), (511), and (440) of the face-centered cubic phase of Co$_3$O$_4$, as identified by JCPDS No. 042–1467. Notably, no evident peaks associated with impurities or alternative phases were discerned, affirming the successful formation of a single-phase Co$_3$O$_4$ material. The FESEM image of the prepared Co$_3$O$_4$ is shown in Figure 4(ciii). The resulting sample presents a porous nanostructure consisting of spheroidal nanoparticles with diameters between 10 and 30 nm. The formation of this porous nanorod gives it a larger surface area, enhancing its ability to sense ethylene. The gas response of the product is shown in Figure 4(civ). It depicts the dynamic resistance of the sensor under the influence of pulses with varying ethylene concentrations, all conducted at the optimized working temperature of 250 °C. The sensor showcases remarkable sensitivity and responsiveness, facilitating the precise detection of even minute quantities of ethylene. Furthermore, the sensor displays commendable recovery performance after exposure to ethylene. Thus, the Co$_3$O$_4$-based ethylene sensor prepared by hydrothermal method shows good performance.

The advantages and disadvantages of the above fabrication methods are summarized in Table 1. Among these methods, CVD, wet chemical method, and electrochemical deposition are more suitable for agricultural applications. As a sensor applied to the agricultural field, it needs to have the characteristics of low price, high production efficiency, and stable performance. These methods are capable of producing high-quality, uniform films or structures to ensure consistency and stability of sensor performance. Next, we will review the MOS-based chemo-resistive ethylene sensors applied in agriculture, which are fabricated by CVD, electrochemical deposition, and wet chemical methods.

Table 1. The summary of the fabrication methods.

Fabrication Methods	Advantages	Disadvantages	Applicable MOSs	Used in Agriculture	Refs.
CVD	High controllability	Limited material applicability	SnO_2	Yes	[43,44]
USP	Stable coatings	Difficult operation	SnO_2	No	[48,51]
Sputtering method	Repeatability	High cost	SnO_2, ZnO	No	[52,53]
Wet chemical method	Complex structure	Limited production	ZnO, Fe_2O_3	Yes	[59]
Electrochemical deposition	Low-temperature conditions	Doping impurity	ZnO	Yes	[63]
Reflux method	Uniform particle	Long reaction time	TiO_2	No	[29]
Hydrothermal method	High crystallinity	Complicated process	Co_3O_4	No	[66]

3. Applications in Agriculture

Nowadays, MOS-based chemo-resistive ethylene sensors are applied in agriculture, which can significantly increase production efficiency and quality. Fruit quality detection, fruit freshness assessment, and banana maturity detection have been performed using chemo-resistive ethylene sensors based on SnO_2 and ZnO.

3.1. Pd-Loaded SnO_2 Sensor for Fruit Maturity Detection

Zhao et al. proposed a chemo-resistive ethylene sensor based on Pd-loaded SnO_2 [70]. The sensor exhibited excellent detection performance, such as a low detection limit (50 ppb), good sensitivity (0.58 ppm^{-1}), and excellent response time (1 s). Then, the researchers further explored the application of this sensor in fruit maturity detection. Four fruits (banana, lemon, apple, and pear) were separately placed in four transparent bottles, and the sensors were inserted into the bottles to real-time detect the ethylene released by the fruits (Figure 5(ai)). The response curve of different fruits shows a large variability. According to the response, the banana released the most ethylene while the apple released the least. In addition, sensor response curves were explored for different numbers of bananas (Figure 5(aii)). We can see that the response of this sensor shows a non-uniform rise with the number of bananas, which was relatively slow at first but became fast when the number of bananas surpassed 4. This effect indicates that ethylene emissions are mutually reinforcing [2]. To further explore the potential application of this sensor in fruit storage, they also looked at how the sensors respond to a banana (Figure 5(aiii)) and a lemon (Figure 5(aiv)) at different stages of ripeness. According to the response curve, we can see that the response of the sensor to the banana first rises fast and then drops, and the transition happens at the climacteric period. The reason for this result is that banana, as a respiratory climacteric fruit, is easily affected by the ethylene concentration in the process of senescence and metamorphosis. In contrast, lemon, as a non-respiratory climacteric fruit, has a relatively slow metabolism and is not easily affected by ethylene concentration. This result also suggests that lemon is more storable than banana. These curves demonstrate the great potential of Pd-loaded SnO_2 ethylene sensors in estimating different species, quantities, and storage states of fruits.

3.2. Cr_2O_3-Tailored SnO_2 Sensor for Fruit Maturity Detection

Recently, a new SnO_2 sensor coated with the nanoscale catalytic Cr_2O_3 overlayer has been proposed in the literature [71]. Notably, the Cr_2O_3 overlayer has little or no oxidizing effect on the relatively stable ethylene but promotes the oxidation of the more reactive interfering gases, resulting in high ethylene selectivity. Moreover, the sensor has a low detection limit of 24 ppb. The researchers evaluated the sensor's potential for detecting fruit ripeness. Five fruits (banana, apple mango, peach, kiwifruit, and blueberry) were separately placed in airtight containers, and the sensor responses to ethylene released from the fruits were monitored for 15 days (Figure 5(bi)). The response curves are shown in Figure 5(bii–vi). The response to ethylene increased as the fruit aged, which proves

the increment in ethylene concentration. In general, banana, apple mango, and peach produced higher amounts of ethylene than the other two fruits, which is associated with whether the fruits are respiratory climacteric. During the monitoring process, the appearance of the peach, kiwifruit, and blueberry did not change significantly, but the ethylene content changed. Therefore, fruit maturity can be assessed by measuring the ethylene concentration before a visible appearance change. For real-time and on-site detection, researchers have developed a portable sensing module that connects wirelessly to cell phones (Figure 5(bvii,viii)), which successfully differentiated three bananas with different maturity levels.
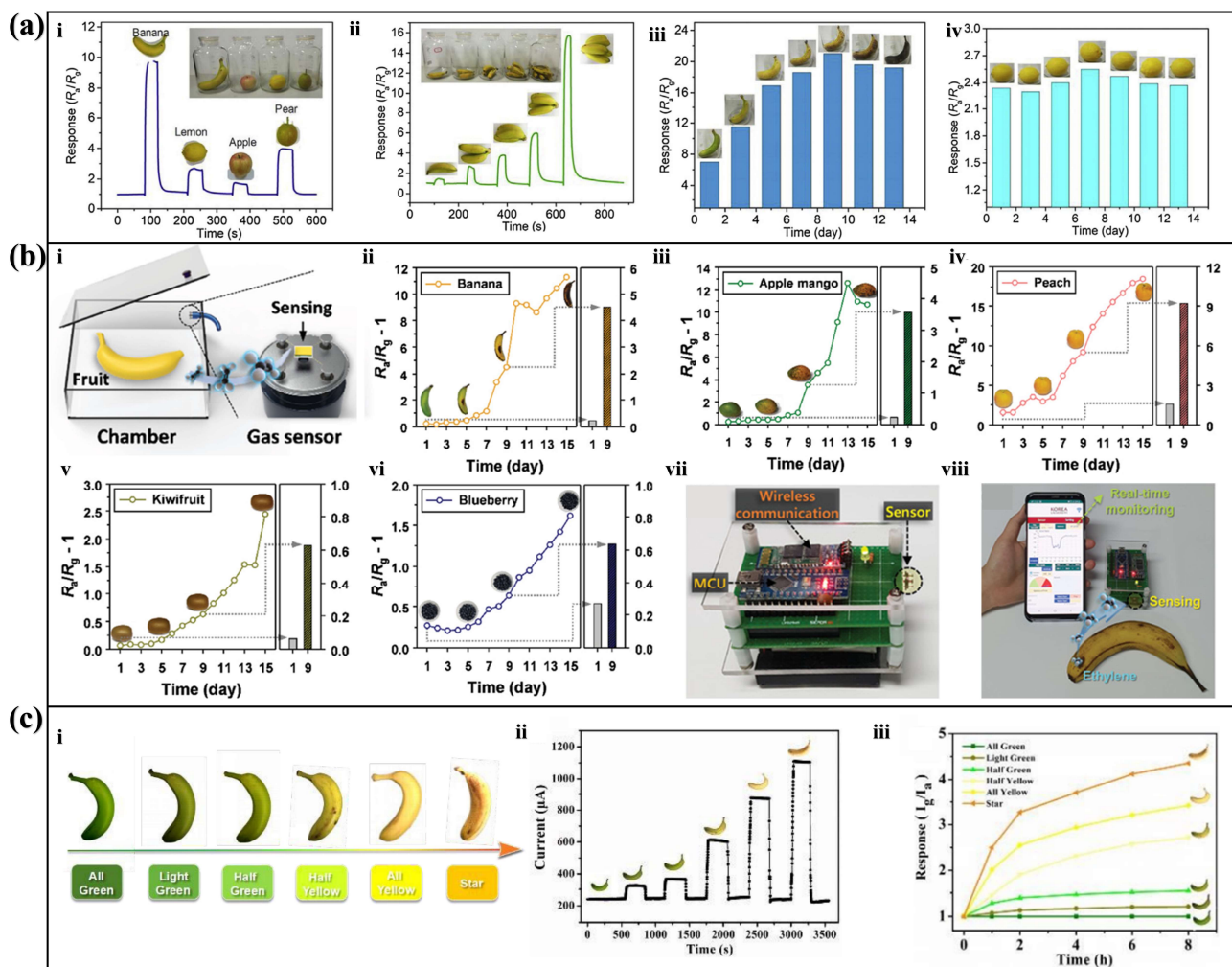
Figure 5. Applications in agriculture. (**a**) Pd-loaded SnO$_2$ sensor for fruit maturity detection: (**i**) The real-time response curves of the gas sensor to four fresh fruits, (**ii**) The response curve of banana with increasing numbers of bananas, and (**iii,iv**) The response to banana and lemon over time [70]. (**b**) Cr$_2$O$_3$-tailored SnO$_2$ sensor for fruit maturity detection: (**i**) Schematic diagram of the detection scene, (**ii–vi**) changes in response to the banana, apple mango, peach, kiwifruit, blueberry; (**vii**) Integrated inspection systems; and (**viii**) Online monitoring photo [71]. (**c**) ZnO nanosheet sensor for banana maturity detection: (**i**) Bananas at different ripeness stages, (**ii**) The real-time response of the sensor to the banana during ripeness process, and (**iii**) The response of the sensor to bananas beginning at different maturity stages over time [72].

3.3. ZnO Nanosheet Sensor for Banana Maturity Detection

Wang et al. fabricated a ZnO nanosheet sensor with good sensing performance and response speed for ethylene detection [72]. Researchers explored the potential of sensors for detecting fruit ripeness using bananas as an example. Six bananas of different ripeness

levels (represented by color, i.e., all green, light green, half green, half yellow, all yellow, star) were placed in sealed containers separately (Figure 5(ci)). The gases in the containers were extracted using a syringe and detected by the sensor. The real-time response of the sensor to the banana during the ripeness process is shown in Figure 5(cii). We can see that the current of the sensor increases rapidly after exposure to ethylene. Moreover, the response of the sensor increases rapidly as the ripeness level increases. The response of the sensor to bananas of different maturity stages over time was also tested (Figure 5(ciii)). This suggests that the ethylene released by bananas first increased and then stabilized. As maturity increased, ethylene was released in greater quantities and at a faster rate. This proves that banana ripeness can be assessed by measuring the ethylene released from the bananas.

4. Sensing Mechanisms

MOS-based chemo-resistive gas sensors mainly use tin dioxide (SnO_2), zinc oxide (ZnO), and others—including titanium dioxide (TiO_2), iron trioxide (Fe_2O_3), and cobalt oxide (Co_3O_4)—as sensing materials [73–82]. According to carriers, MOSs are divided into n-type (electron-dominated), such as SnO_2, ZnO, TiO_2, and Fe_2O_3, and p-type (hole-dominated), such as Co_3O_4. MOS-based chemo-resistive ethylene sensors determine the ethylene concentrations via a resistance change [83]. The detection mechanism of the MOS-based chemo-resistive ethylene sensor is shown in Figure 6. When exposed to atmospheric conditions, oxygen molecules are chemically adsorbed on the surface of the MOS sensing layer. By trapping electrons in the conduction band, the oxygen molecules are converted to chemisorbed oxygen with negative charges, such as O_2^-, O^-, and O^{2-}. The process of chemisorbed oxygen formation can be expressed by the following equations:

$$O_2 + 2e^- \leftrightarrow 2O^- \tag{1}$$

$$O_2 + e^- \leftrightarrow O_2^- \tag{2}$$

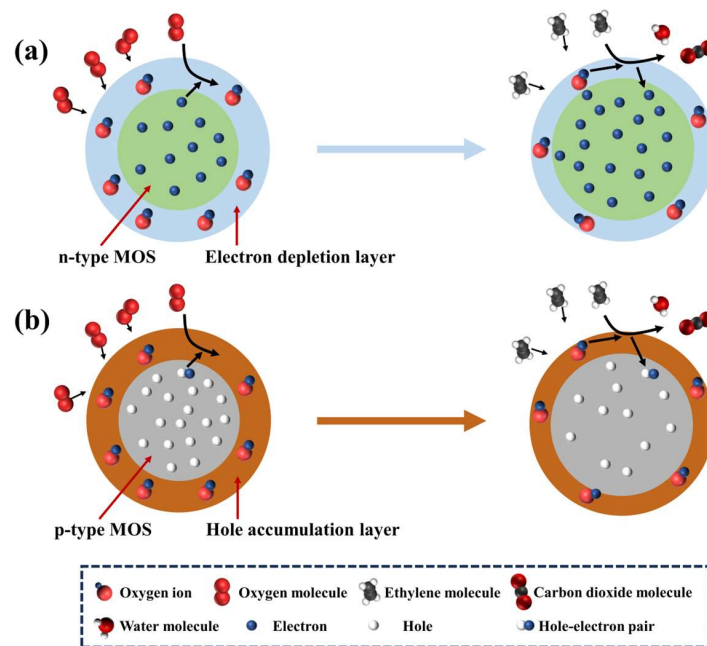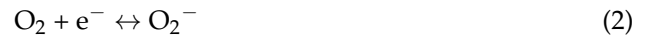$$O^- + e^- \leftrightarrow O^{2-} \tag{3}$$

Figure 6. Sensing mechanisms of chemo-resistive ethylene sensors based on (**a**) n-type and (**b**) p-type MOSs.

Due to the chemisorption of oxygen, an electronic depletion layer (EDL) with low electron concentration is formed on the surface of n-type semiconductors, and a hole

accumulation layer is formed on the surface of p-type semiconductors [83–86]. When exposed to ethylene, a type of reducing gas, ethylene molecules are adsorbed on the surface of the semiconductor sensing layer. The ethylene molecules react with chemisorbed oxygen and release electrons. Taking O^- as an example, the reaction process is as follows:

$$C_2H_4 + 5O^- \leftrightarrow 2CO_2 + 2H_2O + 5e^- \tag{4}$$
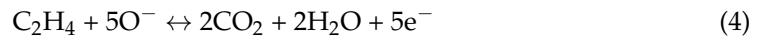
The electrons are released to the sensing layer. For n-type semiconductors, an increase in the electron concentration leads to a thinning of the EDL and a decrease in resistance, while for p-type semiconductors, an increase in the electron concentration leads to a decrease in the number of holes, which leads to a thinning of the hole accumulation layer and the rise in resistance. As the ethylene concentration rises, the amount of resistance change ($|R_a - R_g|/R_a$) increases, in which R_a and R_g represent resistances in the atmosphere and in ethylene gas, respectively. $|R_a - R_g|/R_a$ is typically defined as the response of the sensor, though R_a/R_g and $|R_a - R_g|/R_g$ are also used. Consequently, the ethylene concentration can be derived from the resistance change [9]. Most ethylene sensors are based on n-type MOSs. The above mechanisms can also be applied to other reducing gases, which could lead to a selectivity problem. In the next section, we will discuss this problem and propose possible solutions.

5. Challenges and Perspectives

MOS-based chemo-resistive ethylene sensors demonstrate the advantages of in situ detection, simple miniaturization [26], and cost-effective production [27], which makes them particularly suitable for agricultural applications [20,87]. However, the current applications in agriculture are restricted to the monitoring of ripeness of post-harvest fruits, mainly attributed to six challenges [88], including low selectivity, poor limit of detection, high operation temperature, low anti-humidity capability, long-term stability and sensor drift, and sensor discreteness. Thus, in this paper, we summarize the challenges and provide potential solutions (Figure 7).
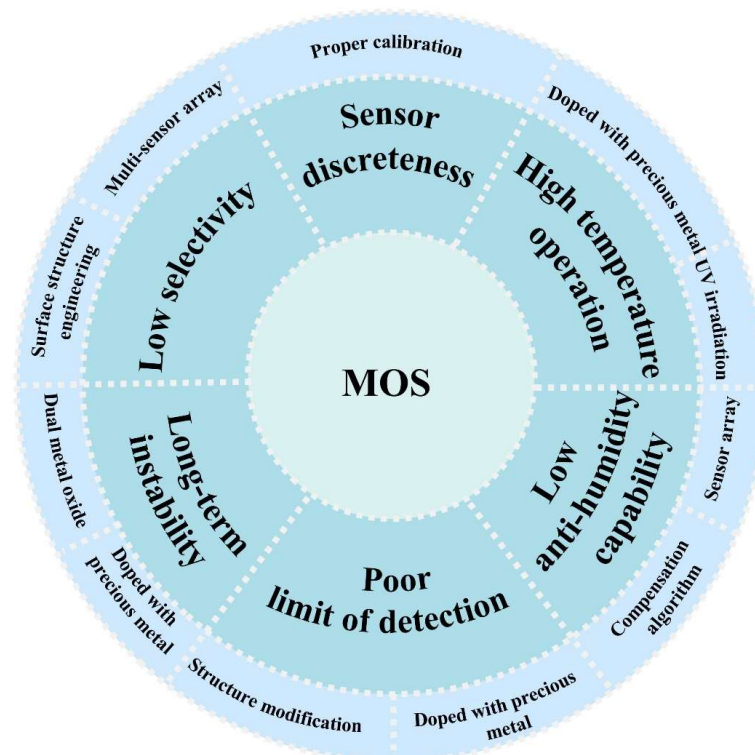

Figure 7. Challenges and potential solutions of MOS-based chemo-resistive ethylene sensors.

1. Low selectivity. MOS-based chemo-resistive gas sensors are susceptible to multiple gases, such as ethane mentioned in Section 2.2.3, which interfere with the detection of ethylene. In particular, the complex composition of gases in agricultural environments, such as water vapor, ethanol, ammonia, and nitrous oxide, makes accurate detection of ethylene a huge challenge. In order to eliminate the interference of non-target gas, we can perform surface structure engineering on the gas-sensitive layer, such as coating microchannels to block interfering gas molecules from reaching the sensing layer [89]. In addition, utilizing the multi-sensor array is also an effective way to combine the response result of multiple sensors to identify ethylene concentrations [90].

2. Poor limit of detection. The limit of detection refers to the lowest concentration of ethylene that the sensor can reliably detect and measure. In the field of agriculture, trace amounts of ethylene can have a large impact on the growth and ripeness of fruits and plants. In addition, the ethylene content in agriculture is usually at the ppb level. It is important to optimize the limit of detection of ethylene sensors [91]. A possible solution is structure modification, such as creating a porous structure to increase the surface area, which can effectively reduce the limit of detection. In addition, doping with precious metals is also an effective strategy [61].

3. High-temperature operation. Due to the inherent nature of ethylene, ethylene sensors typically need to operate at high temperatures (such as 250 °C [70], 300 °C [49], and 350 °C [71]). The high temperature can easily cause damage to the surface of the detection object, limiting its application on plant surfaces and other scenes [72]. Also, the high temperature of the sensor puts higher requirements on the stability of the sensor. Moreover, considering the long working time of the ethylene sensor, the high working temperature also greatly increases the energy consumption. To solve this problem, doping with noble metals is an effective strategy, which acts as catalysts that can effectively reduce the activation energy of ethylene molecules and significantly reduce the working temperature. In addition, UV irradiation can energize the sensors, which can also lower the operating temperature [50].

4. Low anti-humidity capability. Water vapor decreases the sensitivity of the sensor to ethylene gas because water molecules compete with ethylene molecules for oxygen species and reduce the available surface area for the adsorption of ethylene molecules on the MOx surface. Therefore, an increase in humidity decreases the sensitivity of the sensor to ethylene gas. By using a temperature and humidity compensation algorithm, the sensor output can be corrected based on the temperature and humidity information of the environment, thus reducing the effect of humidity on sensor sensitivity. Additionally, it is possible to use the humidity sensor in conjunction with a target gas sensor [92].

5. Long-term instability. In the process of measuring ethylene, in reality, the concentration is often too low. Because the sensors at this stage are still not very sensitive to low concentrations of ethylene, the results will be unstable when measuring. Possible solutions to this issue are doping with precious metals or using bimetallic oxide-based sensors. Precious metals can act as catalysts. Bimetallic oxides increase the specific surface area of the material and thus provide more active sites. These improved methods make the sensor show high stability, even at a low-concentration detection [93].

6. Sensor discreteness. In practice, people find out that even the same series of sensors, due to small differences in the manufacturing process, can lead to slightly different performance between devices. The sensor's working environment and long-term use or aging may also cause the performance of the sensor to change. The sensitivity, response time and other characteristics of the sensor may change with the change of these factors, resulting in the response difference of the sensor under the same conditions. This challenge may (at least partially) be overcome by proper calibration.

6. Conclusions

In summary, we have systematically reviewed the materials, fabrications, applications in agriculture, and sensing mechanisms of MOS-based chemo-resistive sensors. The sensing mechanisms vary depending on the conduction type. The two mainly used MOSs (SnO_2 and ZnO) and others are typically fabricated by CVD, USP, sputtering, wet chemical method, electrochemical deposition, reflux method, and hydrothermal method. The MOS-based chemo-resistive sensors are typically used to monitor the ripeness of fruits in agriculture. Compared to traditional ethylene detection technologies, MOS-based chemo-resistive ethylene sensors have advantages such as low cost and on-site monitoring and are particularly suitable for agricultural applications. Despite these advantages, MOS-based chemo-resistive ethylene sensors are currently restricted to the monitoring of ripeness of post-harvest fruits in agriculture, mainly due to six challenges, including low selectivity, poor limit of detection, high operation temperature, low anti-humidity capability, long-term instability, and sensor discreteness. Accordingly, we have proposed reasonable solutions to address these challenges. With the continuous advancement in MOS-based chemo-resistive ethylene sensors, their applications will be significantly extended, not only in agriculture but also in other fields.

References

1. Saltveit, M.E. Effect of ethylene on quality of fresh fruits and vegetables. *Postharvest Biol. Technol.* **1999**, *15*, 279–292. [CrossRef]
2. Barry, C.S.; Giovannoni, J.J. Ethylene and fruit ripening. *J. Plant Growth Regul.* **2007**, *26*, 143–159. [CrossRef]
3. Pratt, H.K.; Goeschl, J. Physiological roles of ethylene in plants. *Annu. Rev. Plant Physiol.* **1969**, *20*, 541–584. [CrossRef]
4. Bapat, V.A.; Trivedi, P.K.; Ghosh, A.; Sane, V.A.; Ganapathi, T.R.; Nath, P. Ripening of fleshy fruit: Molecular insight and the role of ethylene. *Biotechnol. Adv.* **2010**, *28*, 94–107. [CrossRef]
5. Bleecker, A.B.; Kende, H. Ethylene: A gaseous signal molecule in plants. *Annu. Rev. Cell Dev. Biol.* **2000**, *16*, 1–18. [CrossRef]
6. Bailén, G.; Guillén, F.; Castillo, S.; Serrano, M.; Valero, D.; Martínez-Romero, D. Use of activated carbon inside modified atmosphere packages to maintain tomato fruit quality during cold storage. *J. Agric. Food Chem.* **2006**, *54*, 2229–2235. [CrossRef]
7. Warton, M.; Wills, R.; Ku, V. Ethylene levels associated with fruit and vegetables during marketing. *Aust. J. Exp. Agric.* **2000**, *40*, 465–470. [CrossRef]
8. Kader, A.A. A perspective on postharvest horticulture (1978–2003). *HortScience* **2003**, *38*, 1004–1008. [CrossRef]
9. Hu, B.; Sun, D.-W.; Pu, H.; Wei, Q. Recent advances in detecting and regulating ethylene concentrations for shelf-life extension and maturity control of fruit: A review. *Trends Food Sci. Technol.* **2019**, *91*, 66–82. [CrossRef]
10. Wang, Y.; Diao, P.; Kong, L.; Yu, R.; Zhang, M.; Zuo, T.; Fan, Y.; Niu, Y.; Yan, F.; Wuriyanghan, H. Ethylene enhances seed germination and seedling growth under salinity by reducing oxidative stress and promoting chlorophyll content via ETR2 pathway. *Front. Plant Sci.* **2020**, *11*, 1066. [CrossRef]

11. Swarup, R.; Perry, P.; Hagenbeek, D.; Van Der Straeten, D.; Beemster, G.T.; Sandberg, G.; Bhalerao, R.; Ljung, K.; Bennett, M.J. Ethylene upregulates auxin biosynthesis in Arabidopsis seedlings to enhance inhibition of root cell elongation. *Plant Cell* **2007**, *19*, 2186–2196. [CrossRef]

12. Iqbal, N.; Khan, N.A.; Ferrante, A.; Trivellini, A.; Francini, A.; Khan, M. Ethylene role in plant growth, development and senescence: Interaction with other phytohormones. *Front. Plant Sci.* **2017**, *8*, 475. [CrossRef]

13. Lelièvre, J.M.; Latchè, A.; Jones, B.; Bouzayen, M.; Pech, J.C. Ethylene and fruit ripening. *Physiol. Plant.* **1997**, *101*, 727–739. [CrossRef]

14. Matilla, A.J. Ethylene in seed formation and germination. *Seed Sci. Res.* **2000**, *10*, 111–126. [CrossRef]

15. Ecker, J.R.; Davis, R.W. Plant defense genes are regulated by ethylene. *Proc. Natl. Acad. Sci. USA* **1987**, *84*, 5202–5206. [CrossRef]

16. Adams, D.; Yang, S. Ethylene biosynthesis: Identification of 1-aminocyclopropane-1-carboxylic acid as an intermediate in the conversion of methionine to ethylene. *Proc. Natl. Acad. Sci. USA* **1979**, *76*, 170–174. [CrossRef]

17. Keller, N.; Ducamp, M.-N.; Robert, D.; Keller, V. Ethylene removal and fresh product storage: A challenge at the frontiers of chemistry. Toward an approach by photocatalytic oxidation. *Chem. Rev.* **2013**, *113*, 5029–5070. [CrossRef] [PubMed]

18. Jedermann, R.; Behrens, C.; Westphal, D.; Lang, W. Applying autonomous sensor systems in logistics—Combining sensor networks, RFIDs and software agents. *Sens. Actuators A Phys.* **2006**, *132*, 370–375. [CrossRef]

19. Cristescu, S.M.; Mandon, J.; Arslanov, D.; De Pessemier, J.; Hermans, C.; Harren, F.J. Current methods for detecting ethylene in plants. *Ann. Bot.* **2013**, *111*, 347–360. [CrossRef]

20. Caprioli, F.; Quercia, L. Ethylene detection methods in post-harvest technology: A review. *Sens. Actuators B Chem.* **2014**, *203*, 187–196. [CrossRef]

21. McDonagh, C.; Burke, C.S.; MacCraith, B.D. Optical chemical sensors. *Chem. Rev.* **2008**, *108*, 400–422. [CrossRef]

22. Manne, J.; Jäger, W.; Tulip, J. Sensitive detection of ammonia and ethylene with a pulsed quantum cascade laser using intra and interpulse spectroscopic techniques. *Appl. Phys. B* **2009**, *94*, 337–344. [CrossRef]

23. Scotoni, M.; Rossi, A.; Bassi, D.; Buffa, R.; Iannotta, S.; Boschetti, A. Simultaneous detection of ammonia, methane and ethylene at 1.63 μm with diode laser photoacoustic spectroscopy. *Appl. Phys. B* **2006**, *82*, 495–500. [CrossRef]

24. Kathirvelan, J.; Vijayaraghavan, R. Review on sensitive and selective ethylene detection methods for fruit ripening application. *Sens. Rev.* **2020**, *40*, 421–435. [CrossRef]

25. Zhang, D.; Yang, Z.; Yu, S.; Mi, Q.; Pan, Q. Diversiform metal oxide-based hybrid nanostructures for gas sensing with versatile prospects. *Coord. Chem. Rev.* **2020**, *413*, 213272. [CrossRef]

26. Simon, I.; Bârsan, N.; Bauer, M.; Weimar, U. Micromachined metal oxide gas sensors: Opportunities to improve sensor performance. *Sens. Actuators B Chem.* **2001**, *73*, 1–26. [CrossRef]

27. Hagleitner, C.; Hierlemann, A.; Lange, D.; Kummer, A.; Kerness, N.; Brand, O.; Baltes, H. Smart single-chip gas sensor microsystem. *Nature* **2001**, *414*, 293–296. [CrossRef] [PubMed]

28. Esser, B.; Schnorr, J.M.; Swager, T.M. Selective detection of ethylene gas using carbon nanotube-based devices: Utility in determination of fruit ripeness. *Angew. Chem. Int. Ed.* **2012**, *51*, 5752–5756. [CrossRef]

29. Kathirvelan, J.; Vijayaraghavan, R.; Thomas, A. Ethylene detection using TiO_2–WO_3 composite sensor for fruit ripening applications. *Sens. Rev.* **2017**, *37*, 147–154. [CrossRef]

30. Zanolli, Z.; Leghrib, R.; Felten, A.; Pireaux, J.-J.; Llobet, E.; Charlier, J.-C. Gas sensing with Au-decorated carbon nanotubes. *ACS Nano* **2011**, *5*, 4592–4599. [CrossRef]

31. Garg, N.; Deep, A.; Sharma, A.L. Metal-organic frameworks based nanostructure platforms for chemo-resistive sensing of gases. *Coord. Chem. Rev.* **2021**, *445*, 214073. [CrossRef]

32. Maekawa, T.; Tamaki, J.; Miura, N.; Yamazoe, N. Sensing behavior of CuO-loaded SnO_2 element for H2S detection. *Chem. Lett.* **1991**, *20*, 575–578. [CrossRef]

33. Ishihara, T.; Shiokawa, K.; Eguchi, K.; Arai, H. Selective detection of nitrogen monoxide by the mixed oxide of Cr_2O_3–Nb_2O_5. *Chem. Lett.* **1988**, *17*, 997–1000. [CrossRef]

34. Ishihara, T.; Shiokawa, K.; Egeuchi, K. H, Arai, The mixed oxide A1203-V205 as a semiconductor gas sensor for NO and NO_2. *Sens. Actuators* **1989**, *19*, 259–265. [CrossRef]

35. Ishihara, T.; Matsubara, S. Capacitive type gas sensors. *J. Electroceram.* **1998**, *2*, 215–228. [CrossRef]

36. Bruce, J.; Bosnick, K.; Heidari, E.K. Pd-decorated ZnO nanoflowers as a promising gas sensor for the detection of meat spoilage. *Sens. Actuators B Chem.* **2022**, *355*, 131316. [CrossRef]

37. Tonezzer, M. Single nanowire gas sensor able to distinguish fish and meat and evaluate their degree of freshness. *Chemosensors* **2021**, *9*, 249. [CrossRef]

38. Jang, J.S.; Jung, H.J.; Chong, S.; Kim, D.H.; Kim, J.; Kim, S.O.; Kim, I.D. 2D materials decorated with ultrathin and porous graphene oxide for high stability and selective surface activity. *Adv. Mater.* **2020**, *32*, 2002723. [CrossRef] [PubMed]

39. Jang, J.-S.; Winter, L.R.; Kim, C.; Fortner, J.D.; Elimelech, M. Selective and sensitive environmental gas sensors enabled by membrane overlayers. *Trends Chem.* **2021**, *3*, 547–560. [CrossRef]

40. Ivec, M.; Leitner, R.; Waldner, R.; Gostner, J.; Überall, F. The effect of sensor temperature and MOx layer thickness on the sensitivity of SnO_2-and WO_3-based chemiresistive sensors to ethylene gas. In *Smart Sensors, Actuators, and MEMS VII; and Cyber Physical Systems*; SPIE: Bellingham, WA, USA, 2015; pp. 270–277.

41. Bose, A.C.; Kalpana, D.; Thangadurai, P.; Ramasamy, S. Synthesis and characterization of nanocrystalline SnO_2 and fabrication of lithium cell using nano-SnO_2. *J. Power Sources* **2002**, *107*, 138–141. [CrossRef]

42. Banerjee, R.; Das, D. Properties of tin oxide films prepared by reactive electron beam evaporation. *Thin Solid Films* **1987**, *149*, 291. [CrossRef]

43. Liu, Y.; Zha, S.; Liu, M. Novel Nanostructured Electrodes for Solid Oxide Fuel Cells Fabricated by Combustion Chemical Vapor Deposition (CVD). *Adv. Mater.* **2004**, *16*, 256–260. [CrossRef]

44. Liu, Y.; Zha, S.; Liu, M. Nanocomposite Electrodes Fabricated by a Particle-Solution Spraying Process for Low-Temperature SOFCs. *Chem. Mater.* **2004**, *16*, 3502–3506. [CrossRef]

45. Akhir, M.A.; Mohamed, K.; Rezan, S.A.; Arafat, M.; Haseeb, A.; Uda, M.; Nuradibah, M. Ethylene gas sensing properties of tin oxide nanowires synthesized via CVD method. In Proceedings of the IOP Conference Series: Materials Science and Engineering; IOP Publishing: Bristol, UK, 2018; p. 012038.

46. Akhir, M.A.M.; Mohamed, K.; Rezan, S.A.; Lee, H.L.; Izah, S.S.M. An assessment of chemical vapor deposition synthesis of SnO_2 nanowires by statistical design. *Key Eng. Mater.* **2016**, *701*, 52–56. [CrossRef]

47. Nguyen, T.K.; Yu, S.H.; Yan, J.; Chua, D.H. SnO_2-anchored carbon fibers chemical vapor deposition (CVD) synthesis: Effects of growth parameters on morphologies and electrochemical behaviors. *J. Mater. Sci.* **2020**, *55*, 15588–15601. [CrossRef]

48. Sun, J.; Sun, P.; Zhang, D.; Xu, J.; Liang, X.; Liu, F.; Lu, G. Growth of SnO_2 nanowire arrays by ultrasonic spray pyrolysis and their gas sensing performance. *RSC Adv.* **2014**, *4*, 43429–43435. [CrossRef]

49. Jadsadapattarakul, D.; Thanachayanont, C.; Nukeaw, J.; Sooknoi, T. Improved selectivity, response time and recovery time by [0 1 0] highly preferred-orientation silicalite-1 layer coated on SnO_2 thin film sensor for selective ethylene gas detection. *Sens. Actuators B Chem.* **2010**, *144*, 73–80. [CrossRef]

50. Ahn, H.; Noh, J.H.; Kim, S.-B.; Overfelt, R.A.; Yoon, Y.S.; Kim, D.-J. Effect of annealing and argon-to-oxygen ratio on sputtered SnO_2 thin film sensor for ethylene gas detection. *Mater. Chem. Phys.* **2010**, *124*, 563–568. [CrossRef]

51. Ardekani, S.R.; Aghdam, A.S.R.; Nazari, M.; Bayat, A.; Yazdani, E.; Saievar-Iranizad, E. A comprehensive review on ultrasonic spray pyrolysis technique: Mechanism, main parameters and applications in condensed matter. *J. Anal. Appl. Pyrolysis* **2019**, *141*, 104631. [CrossRef]

52. Jamkhande, P.G.; Ghule, N.W.; Bamer, A.H.; Kalaskar, M.G. Metal nanoparticles synthesis: An overview on methods of preparation, advantages and disadvantages, and applications. *J. Drug Deliv. Sci. Technol.* **2019**, *53*, 101174. [CrossRef]

53. Abid, N.; Khan, A.M.; Shujait, S.; Chaudhary, K.; Ikram, M.; Imran, M.; Haider, J.; Khan, M.; Khan, Q.; Maqbool, M. Synthesis of nanomaterials using various top-down and bottom-up approaches, influencing factors, advantages, and disadvantages: A review. *Adv. Colloid Interface Sci.* **2022**, *300*, 102597. [CrossRef] [PubMed]

54. Kang, Y.; Yu, F.; Zhang, L.; Wang, W.; Chen, L.; Li, Y. Review of ZnO-based nanomaterials in gas sensors. *Solid State Ion.* **2021**, *360*, 115544. [CrossRef]

55. Wang, Z.L. Splendid one-dimensional nanostructures of zinc oxide: A new nanomaterial family for nanotechnology. *ACS Nano* **2008**, *2*, 1987–1992. [CrossRef] [PubMed]

56. Zheng, J.; Jiang, Z.-Y.; Kuang, Q.; Xie, Z.-X.; Huang, R.-B.; Zheng, L.-S. Shape-controlled fabrication of porous ZnO architectures and their photocatalytic properties. *J. Solid State Chem.* **2009**, *182*, 115–121. [CrossRef]

57. Cui, J.; Jiang, J.; Shi, L.; Zhao, F.; Wang, D.; Lin, Y.; Xie, T. The role of Ni doping on photoelectric gas-sensing properties of ZnO nanofibers to HCHO at room-temperature. *RSC Adv.* **2016**, *6*, 78257–78263. [CrossRef]

58. Zhu, L.; Zeng, W. Room-temperature gas sensing of ZnO-based gas sensor: A review. *Sens. Actuators A Phys.* **2017**, *267*, 242–261. [CrossRef]

59. Chen, J.; Ma, Q.; Wu, X.-J.; Li, L.; Liu, J.; Zhang, H. Wet-chemical synthesis and applications of semiconductor nanomaterial-based epitaxial heterostructures. *Nano-Micro Lett.* **2019**, *11*, 1–28. [CrossRef]

60. Jin, Z.; Wang, D.-C.; Xie, W.-J.; Ding, Y.; Li, J. Highly Sensitive Ethylene Sensors Based on Ultrafine Pd Nanoparticles-Decorated Porous ZnO Nanosheets and Their Application in Fruit Ripeness Detection. *Processes* **2023**, *11*, 1686. [CrossRef]

61. Sholehah, A.; Karmala, K.; Huda, N.; Utari, L.; Septiani, N.L.W.; Yuliarto, B. Structural effect of ZnO-Ag chemoresistive sensor on flexible substrate for ethylene gas detection. *Sens. Actuators A Phys.* **2021**, *331*, 112934. [CrossRef]

62. Aldosary, A.F.; Shar, M.A.; AlQahtani, H.R. High-sensitivity detection of ethane and ethylene using gamma-irradiated ZnO chemiresistors. *Meas. Sens.* **2022**, *24*, 100600. [CrossRef]

63. Liu, L.; Mandler, D. Using nanomaterials as building blocks for electrochemical deposition: A mini review. *Electrochem. Commun.* **2020**, *120*, 106830. [CrossRef]

64. Sholehah, A.; Faroz, D.F.; Huda, N.; Utari, L.; Septiani, N.L.W.; Yuliarto, B. Synthesis of ZnO flakes on flexible substrate and its application on ethylene sensing at room temperature. *Chemosensors* **2019**, *8*, 2. [CrossRef]

65. Tesfamichael, T.; Cetin, C.; Piloto, C.; Arita, M.; Bell, J. The effect of pressure and W-doping on the properties of ZnO thin films for NO2 gas sensing. *Appl. Surf. Sci.* **2015**, *357*, 728–734. [CrossRef]

66. Li, B.; Li, M.; Meng, F.; Liu, J. Highly sensitive ethylene sensors using Pd nanoparticles and rGO modified flower-like hierarchical porous α-Fe_2O_3. *Sens. Actuators B Chem.* **2019**, *290*, 396–405. [CrossRef]

67. Ma, C.Y.; Mu, Z.; Li, J.J.; Jin, Y.G.; Cheng, J.; Lu, G.Q.; Hao, Z.P.; Qiao, S.Z. Mesoporous Co_3O_4 and Au/Co_3O_4 catalysts for low-temperature oxidation of trace ethylene. *J. Am. Chem. Soc.* **2010**, *132*, 2608–2613. [CrossRef] [PubMed]

68. Gholami, M.; Bahar, M.; Azim-Araghi, M. The preparation of TiO_2 nanoparticles and investigation of its electrical properties as CO_2 gas sensor at room temperature. *Chem. Phys. Lett.* **2012**, *48*, 9626–9628.

69. Le Dang, T.T.; Do, T.N.T.; Tonezzer, M.; Tran, V.D.N.; Chu, T.X.; Chu, M.H.; Nguyen, D.H. Eco-friendly facile synthesis of Co$_3$O$_4$–Pt nanorods for ethylene detection towards fruit quality monitoring. *Sens. Actuators A Phys.* **2023**, *362*, 114607. [CrossRef]

70. Zhao, Q.; Duan, Z.; Yuan, Z.; Li, X.; Si, W.; Liu, B.; Zhang, Y.; Jiang, Y.; Tai, H. High performance ethylene sensor based on palladium-loaded tin oxide: Application in fruit quality detection. *Chin. Chem. Lett.* **2020**, *31*, 2045–2049. [CrossRef]

71. Jeong, S.Y.; Moon, Y.K.; Kim, T.H.; Park, S.W.; Kim, K.B.; Kang, Y.C.; Lee, J.H. A new strategy for detecting plant hormone ethylene using oxide semiconductor chemiresistors: Exceptional gas selectivity and response tailored by nanoscale Cr$_2$O$_3$ catalytic overlayer. *Adv. Sci.* **2020**, *7*, 1903093. [CrossRef]

72. Wang, L.-P.; Jin, Z.; Luo, T.; Ding, Y.; Liu, J.-H.; Wang, X.-F.; Li, M.-Q. The detection of ethylene using porous ZnO nanosheets: Utility in the determination of fruit ripeness. *New J. Chem.* **2019**, *43*, 3619–3624. [CrossRef]

73. Eom, T.H.; Cho, S.H.; Suh, J.M.; Kim, T.; Yang, J.W.; Lee, T.H.; Jun, S.E.; Kim, S.J.; Lee, J.; Hong, S.H. Visible Light Driven Ultrasensitive and Selective NO$_2$ Detection in Tin Oxide Nanoparticles with Sulfur Doping Assisted by l-Cysteine. *Small* **2022**, *18*, 2106613. [CrossRef] [PubMed]

74. Kim, T.H.; Hasani, A.; Kim, Y.; Park, S.Y.; Lee, M.G.; Sohn, W.; Nguyen, T.P.; Choi, K.S.; Kim, S.Y.; Jang, H.W. NO$_2$ sensing properties of porous Au-incorporated tungsten oxide thin films prepared by solution process. *Sens. Actuators B Chem.* **2019**, *286*, 512–520. [CrossRef]

75. Kim, Y.; Kwon, K.C.; Kang, S.; Kim, C.; Kim, T.H.; Hong, S.-P.; Park, S.Y.; Suh, J.M.; Choi, M.-J.; Han, S. Two-dimensional NbS$_2$ gas sensors for selective and reversible NO$_2$ detection at room temperature. *ACS Sens.* **2019**, *4*, 2395–2402. [CrossRef] [PubMed]

76. Park, S.-W.; Jeong, S.-Y.; Moon, Y.K.; Kim, K.; Yoon, J.-W.; Lee, J.-H. Highly selective and sensitive detection of breath isoprene by tailored gas reforming: A synergistic combination of macroporous WO$_3$ spheres and Au catalysts. *ACS Appl. Mater. Interfaces* **2022**, *14*, 11587–11596. [CrossRef] [PubMed]

77. Bulemo, P.M.; Kim, I.-D. Recent advances in ABO$_3$ perovskites: Their gas-sensing performance as resistive-type gas sensors. *J. Korean Ceram. Soc.* **2020**, *57*, 24–39. [CrossRef]

78. Kim, T.-H.; Yoon, J.-W.; Lee, J.-H.; Kim, T.-H.; Yoon, J.-W.; Lee, J.-H. A volatile organic compound sensor using porous Co$_3$O$_4$ spheres. *J. Korean Ceram. Soc.* **2016**, *53*, 134–138. [CrossRef]

79. Andrysiewicz, W.; Krzeminski, J.; Skarżynski, K.; Marszalek, K.; Sloma, M.; Rydosz, A. Flexible gas sensor printed on a polymer substrate for sub-ppm acetone detection. *Electron. Mater. Lett.* **2020**, *16*, 146–155. [CrossRef]

80. Cho, S.H.; Suh, J.M.; Eom, T.H.; Kim, T.; Jang, H.W. Colorimetric sensors for toxic and hazardous gas detection: A review. *Electron. Mater. Lett.* **2021**, *17*, 1–17. [CrossRef]

81. Eom, T.H.; Cho, S.H.; Suh, J.M.; Kim, T.; Lee, T.H.; Jun, S.E.; Yang, J.W.; Lee, J.; Hong, S.-H.; Jang, H.W. Substantially improved room temperature NO$_2$ sensing in 2-dimensional SnS$_2$ nanoflowers enabled by visible light illumination. *J. Mater. Chem. A* **2021**, *9*, 11168–11178. [CrossRef]

82. Lee, C.W.; Suh, J.M.; Choi, S.; Jun, S.E.; Lee, T.H.; Yang, J.W.; Lee, S.A.; Lee, B.R.; Yoo, D.; Kim, S.Y. Surface-tailored graphene channels. *Npj 2D Mater. Appl.* **2021**, *5*, 39. [CrossRef]

83. Wang, C.; Yin, L.; Zhang, L.; Xiang, D.; Gao, R. Metal oxide gas sensors: Sensitivity and influencing factors. *Sensors* **2010**, *10*, 2088–2106. [CrossRef]

84. Barsan, N.; Koziej, D.; Weimar, U. Metal oxide-based gas sensor research: How to? *Sens. Actuators B Chem.* **2007**, *121*, 18–35. [CrossRef]

85. Matsunaga, N.; Sakai, G.; Shimanoe, K.; Yamazoe, N. Diffusion equation-based study of thin film semiconductor gas sensor-response transient. *Sens. Actuators B Chem.* **2002**, *83*, 216–221. [CrossRef]

86. Park, S.Y.; Kim, Y.; Kim, T.; Eom, T.H.; Kim, S.Y.; Jang, H.W. Chemoresistive materials for electronic nose: Progress, perspectives, and challenges. *InfoMat* **2019**, *1*, 289–316. [CrossRef]

87. Awang, Z. Gas sensors: A review. *Sens. Transducers* **2014**, *168*, 61–75.

88. Presti, D.L.; Di Tocco, J.; Massaroni, C.; Cimini, S.; De Gara, L.; Singh, S.; Raucci, A.; Manganiello, G.; Woo, S.L.; Schena, E. Current understanding, challenges and perspective on portable systems applied to plant monitoring and precision agriculture. *Biosens. Bioelectron.* **2022**, *222*, 115005. [CrossRef] [PubMed]

89. Wusiman, M.; Taghipour, F. Methods and mechanisms of gas sensor selectivity. *Crit. Rev. Solid State Mater. Sci.* **2022**, *47*, 416–435. [CrossRef]

90. Leangtanom, P.; Wisitsoraat, A.; Chanlek, N.; Phanichphant, S.; Kruefu, V. Highly sensitive and selective ethylene gas sensors based on CeOx-SnO$_2$ nanocomposites prepared by a Co-precipitation method. *Mater. Chem. Phys.* **2020**, *254*, 123540. [CrossRef]

91. Giberti, A.; Carotta, M.C.; Guidi, V.; Malagù, C.; Martinelli, G.; Piga, M.; Vendemiati, B. Monitoring of ethylene for agro-alimentary applications and compensation of humidity effects. *Sens. Actuators B Chem.* **2004**, *103*, 272–276. [CrossRef]

92. Krivec, M.; Mc Gunnigle, G.; Abram, A.; Maier, D.; Waldner, R.; Gostner, J.M.; Überall, F.; Leitner, R. Quantitative ethylene measurements with MOx chemiresistive sensors at different relative air humidities. *Sensors* **2015**, *15*, 28088–28098. [CrossRef]

93. Chen, X.; Wreyford, R.; Nasiri, N. Recent Advances in Ethylene Gas Detection. *Materials* **2022**, *15*, 5813. [CrossRef]